Available online at www.sciencedirect.com
ScienceDirect
Journal of the European Ceramic Society 27 (2007) 2183–2193
www.elsevier.com/locate/jeurceramsoc

Densification during hot-pressing of carbon nanotube–metal–magnesium aluminate spinel nanocomposites

A. Peigney *, S. Rul, F. Lefèvre-Schlick, C. Laurent

CIRIMAT, UMR CNRS-UPS-INPT 5085, Centre Interuniversitaire de Recherche et d'Ingénierie des Matériaux, Bât. 2R1, Université Paul-Sabatier, 31062 Toulouse Cedex 9, France

Received 1 April 2006; received in revised form 10 July 2006; accepted 21 July 2006
Available online 18 September 2006

Abstract

The densification by hot-pressing of ceramic–matrix composites containing a dispersion of carbon nanotubes (CNT), mostly single-walled, is studied for the first time. Fifteen different CNT–Co/Mo–$MgAl_2O_4$ composite powders containing between 1.2 and 16.7 vol.% CNT were prepared by catalytic chemical vapour deposition. The in situ growth of CNT within the oxide powder made it possible to obtain a highly homogeneous distribution of CNT. Low contents of CNT (up to 5 vol.%) are beneficial for the first shrinkage step (up to 1100 °C), dominated by the rearrangement process, while higher contents are detrimental. At higher temperatures (1100–1300 °C), CNT clearly inhibit the shrinkage, and this detrimental effect regularly increases with the CNT content. Several explanations are proposed, in relation with the particular mechanical properties of CNT and their highly connected web-like distribution within the material.

Keyword: Hot pressing; Nanocomposites; Spinels ;Carbon nanotubes

1. Introduction

Carbon nanotubes (CNT) have an extremely high aspect ratio (length/diameter well over 1000) and exceptional mechanical, electrical and thermal characteristics, which makes them particularly interesting for use in nanocomposite materials with a metal–matrix, polymer–matrix or ceramic–matrix.[1] However, relatively few works have so far addressed such ceramic–matrix composites. The preparation methods and the obtained properties of CNT–ceramic composites have been extensively reviewed recently.[2] Two of the key problems are the dispersion of the CNT in the matrix and the densification of the composites. Most authors prepared CNT–ceramic composite powders by mixing raw or purified single-walled (SWNT) or multi-walled CNT (MWNT) with the matrix powder or a suitable precursor of the matrix.[3–8] These processes generally require milling during long times to improve the homogeneity, and these treatments necessarily damage CNT. Alternative routes involves composite powders with either CNT grown in situ in a ceramic powder[9–14] or the ceramic synthezised in situ on CNT.[15,16] These processes give rise to most homogeneous dispersions of the two phases and avoid any damage to CNT. Very often, the densification of the composites is conducted by hot-pressing[3,4,7,8,14,17–21] and most of the authors have shown that CNT induce uncomplete densifications, and that this phenomenon increases with the CNT content. Some authors[5,6,22–24] showed that better densifications can be obtained by using the spark plasma sintering (SPS) technique. From most of the works published on the preparation of CNT–ceramic nanocomposites by hot-pressing, it appears that CNT always inhibit the densification of the material, when compared to the corresponding matrix, and that this inhibition is all the more pronounced when the CNT content is increased.

The present authors have reported the synthesis of CNT–Fe–Al_2O_3, CNT–M–$MgAl_2O_4$ and CNT–M–MgO (M = Fe, Co, Ni or alloy) composite powders.[9,12] Because the small diameter CNT as single-, double- and thin multi-walled (SWNT, DWNT and MWNT, respectively) are synthesized in situ in the ceramic powder, their distribution is highly homogeneous. Particularly, when the CNT content is suffiencently high (more than 4–5 vol.%), they form a web-like structure all around the ceramic grain which gives some cohesion to the composite powder. The

* Corresponding author. Tel.: +33 5 61 55 61 55; fax: +33 5 61 55 61 63.
E-mail address: peigney@chimie.ups-tlse.fr (A. Peigney).

0955-2219/$ – see front matter © 2006 Elsevier Ltd. All rights reserved.
doi:10.1016/j.jeurceramsoc.2006.07.012

early studies on the hot-pressing of these very homogeneous composites showed that in comparison to similar carbon-free nanocomposites, the matrix grains are smaller and the relative densities are lower.[18–21] In addition, both with Al_2O_3 and $MgAl_2O_4$ matrix, a fraction of the CNT seems to be destroyed during hot-pressing at 1500 °C in a vacuum. When using the MgO matrix, most CNT are destroyed during a hot-pressing at 1600 °C, but the CNT are not damaged if the treatment is limited to 1200 °C.[20] It seems that the quantity of CNT retained in the massive composite is more dependant on the treatment temperature than on the nature of the oxide matrix. CNT damaging produces disordered graphene (one sheet of graphite structure) layers which gather at matrix grain junctions. Probably owing to a too low relative density (87–93%), the fracture strength and the fracture toughness of the CNT containing composites are generally lower than those of the carbon-free metal oxide composites and only marginally higher than those of the corresponding ceramics.

The present paper reports a study of the densification of 15 different CNT–Co/Mo–$MgAl_2O_4$ composites containing between 1.2 and 16.7 vol.% CNT. In all the composite powders, as shown earlier,[21] CNT are similar and of high quality, 70–90% being SWNT and most of the others being DWNTs, without carbon nanofibres nor significant amount of disordered carbon. The aim is to elucidate the influence of increasing amounts of SWNTs during each of the densification steps of the composites, on hot-pressing. A particular attention has been paid to discriminate between the influence of the CNT and that of other microstructural characteristics of the starting materials.

2. Experimental procedure

The general method for the synthesis of CNT–metal–$MgAl_2O_4$ composite powders which consists in the reduction in a H_2–CH_4 gas mixture of a $Mg_{1-x}Co_xAl_2O_4$ solid solution (catalytic material) was described elsewhere.[11,12,21] During this process, the selective reduction of Co^{II} cations produces Co nanoparticles, no more than a few nanometers in diameter. Those which are located at the oxide grain surface immediately catalyse the decomposition of CH_4 and the subsequent in situ formation of thin diameter CNT. As a result, the CNT are very well distributed all around the oxide grains. In the present work, all the catalytic materials were reduced (CCVD treatment) at 1000 °C (5 °C/min on heating and cooling without any dwell time) in a H_2–CH_4 gas mixture (flow rate 250 sccm) containing 18 mol% CH_4. The flowing gas was dried on P_2O_5 and its composition was regulated by massflow controllers. The control of the quantity of CNT was conducted by varying the composition and the characteristics of the catalytic material. In all, 15 CNT–metal–$MgAl_2O_4$ specimens were prepared, with the CNT content varying over a very wide range (1.2–16.7 vol.%).

Firstly, four $Mg_{1-x}Co_xAl_2O_4$ solid solutions ($x = 0.01$, 0.05, 0.1 and 0.2, respectively) were prepared by the nitrate–urea combustion technique[25] as reported elsewhere.[26] The combustion products were ground manually to powders. These powders are made up of primary grains smaller than 100 nm but strongly aggregated, which required attrition-milling in order to reduce the aggregate size to less than 1 μm. For this operation, 20 g of powder were dispersed in deionised water (28 wt.% of dry matter) containing 0.7 wt.% of dispersant (Duramax D-3005 3005, Rohm and Haas, France), and were then milled by attrition (nylon vessel and rotor, Y-ZrO_2 balls 1 mm in diameter, 2000 rpm, during 2 h 15 min). After attrition-milling, the zirconia balls were separated by rinsing in deionised water and filtering the slurry. A part of each batch was fully dried and calcined at 500 °C to eliminate nylon contamination. Each of the four as-obtained powders was reduced (CCVD treatment) in the form of a powder bed. The so-obtained CNT–Co–$MgAl_2O_4$ composite powders contain from 0.55 to 2.5 wt.% of carbon (specimens C1, C2, C3 and C4—Table 1). Indeed, more Co^{2+} ions in the starting oxide results in more Co catalytic nanoparticles formed upon reduction, which in turn results, after reduction, in higher quantities of CNT. Another part for each batch was only partly evaporated so as to obtain a volume of 100 mL, and used for the preparation of a foam as described later in this section.

Table 1
Composition and preparation route of the starting oxides used for the CCVD synthesis of the CNT–metal–$MgAl_2O_4$ composites and carbon content (C_n) in the composites; proportion of cobalt and molybdenum ions in the starting oxide calculated with respect to the total cation content (cat.%); P, powder; IF, foam prepared by impregnating a polymeric foam with an aqueous suspension of the solid solution powder; GF, foam prepared by a gelcasting-foam method

Specimen	Co (cat.%)	Mo (cat.%)	Preparation route	C_n (wt.%)
C1	1	0	P	0.55
C2	5	0	P	0.6
C3	10	0	P	1.2
C4	20	0	P	2.5
C5	20	0	IF	2.6
C6	20	0	GF	3.7
CM1	10	5	P	4.4
CM2	20	10	P	5.1
CM3	20	5	P	6.4
CM4	20	10	IF	7.0
CM5	10	5	GF	7.2
CM6	20	10	GF	7.3
CM7	5	5	GF	7.5
CM8	20	5	IF	7.8
CM9	20	5	GF	8.0

Secondly, we prepared $Mg_{1-x}Co_xAl_2O_4$ powders ($x = 0.5$, 0.1 and 0.2) containing some MoO_x oxide (5 or 10 cat.% refered to (Mg + Co + Mo)—Table 1)), molybdenum being added via the addition of the desired proportion of ammonium heptamolybdate in the nitrate–urea solution prior to the combustion synthesis. Indeed, it is known that Co/Mo catalysts produce more CNT than Co alone.[27,28] A part of each batch was fully dried and calcined at 500 °C to eliminate nylon contamination. The reduction of three such catalytic materials, with different Co/Mo ratio and (Co + Mo) total contents, in the form of powder beds, produces three CNT–Co/Mo–$MgAl_2O_4$ composites powders (specimens CM1, CM2 and CM3 containing between 4.4 and 6.4 wt.% of carbon—Table 1). Again, another part for each batch was only partly evaporated so as to obtain a volume of 100 mL, and used for the preparation of a foam as described below.

It has been shown that the reduction of a catalytic material in the form of a foam as opposed to a powder bed leads to a significant increase of the CNT content.[26,29] This is the consequence of an easier supply of the H_2–CH_4 gas mixture to the catalytic material. We used several $Mg_{1-x}Co_xAl_2O_4$ powders (containing or not some MoO_x oxide), which were attritor milled, the products being then only partly evaporated. Foams were prepared either by an impregnation route[26] (IF preparation route; Table 1), or by the gelcasting-foam method[29] (GF preparation route; Table 1). The IF route consists in impregnating a commercial polyurethane sponge with a slurry made from the attrited powder followed by drying and calcination steps in order to produce auto-supported $Mg_{1-x}Co_xAl_2O_4$ foams (containing or not some MoO_x oxide). The relative density of the foam is close to 1% and its S_w is similar to that of the starting powder ($35\ m^2\ g^{-1}$). The gelcasting-foam method was described in detail elsewhere.[29] By reduction of the IF and GF foams, a series of other CNT–metal–$MgAl_2O_4$ composites (C5, C6, CM4–CM9; Table 1) were obtained containing more CNT than those obtained by reduction of the corresponding catalytic materials in the form of powder beds.

All specimens are listed in Table 1 by increasing carbon content (up to 8.0 wt.% for CM9), as determined by flash combustion with an accuracy of ±2%. Flash combustion is based on the complete and instantaneous oxidation of carbon into CO_2 which is detected by a thermal conductivity detector, giving an output signal proportional to the concentration in the specimen.

The so-obtained CNT–metal–$MgAl_2O_4$ specimens were firstly uniaxially cold-pressed at 100 MPa in a steel die, and the green density were calculated from their measured weight and dimensions. Then, the green specimens were put in graphite dies, heated up to 900 °C in a secondary vacuum ($P < 10^{-4}$ Torr), at which temperature a pressure of 43 MPa is applied and maintained during the heating up to different temperatures (1200–1500 °C), at a constant heating rate (10 ± 1 °C/min), and during a dwell time of 20 min at the maximum temperature. The shrinkage was followed mechanically and corrected from the dilatation of the graphite column of the apparatus. The so-obtained pellets (10 mm in diameter and 2.5 mm thick) were polished on the two faces and the hot-pressed density was calculated from their measured weight and dimensions. Since hot-pressing was conducted in a secondary vacuum and in a graphite environment, we supposed that the specimens do not lose any carbon during the process. So, the carbon content in the hot-pressed composites was considered to be that of the starting powders. Selected composite powders and the fracture surface of selected hot-pressed composites were observed with a high resolution Field-Effect-Gun Scanning Electron Microscope (FEG-SEM—JEOL JSM 6700F). The observation of the fracture surface of hot-pressed composites gives information about the eventual damage of CNT during sintering, their distribution in the matrix and the approximative size of matrix grains. Polished surfaces were also observed with FEG-SEM but gave only little informations about the microstructures because of the too poor relative density of most specimens and of the submicronic size of most of the matrix grains.

Table 2
Hot-pressing temperature and green and hot-pressed densifications for the 15.5 vol.% CNT–Co/Mo–$MgAl_2O_4$ composite (specimen CM7)

Hot-pressing temperature (°C)	Green densification (%)	Hot-pressed densification (%)
1200	45.0 ± 1.1	74.2 ± 1.9
1300	49.0 ± 1.2	80.2 ± 2.0
1400	45.1 ± 1.1	79.7 ± 2.0
1500	44.0 ± 1.1	85.5 ± 2.1

3. Results and discussion

3.1. Influence of the hot-pressing temperature

The influence of the hot-pressing temperature (1200, 1300, 1400 and 1500 °C) was studied on the CNT–metal–$MgAl_2O_4$ specimen CM7, containing a relatively high quantity (7.5 wt.% or 15.5 vol.% CNT—SEM of the powder in Fig. 2d) and some cobalt (0.73 vol.%) and Mo_2C (1.25 vol.%) nanoparticles (Table 3). The trend is that the hot-pressed densification increases (from 74.2 to 85.5%) upon the increase of the hot-pressing temperature (Table 2). For the specimen hot-pressed at 1300 °C, a higher green densification than expected was obtained, probably caused by a pressure exceeding 100 MPa during the cold-pressing, and results in a HP densification similar to that of the specimen hot-pressed at 1400 °C. FEG-SEM images of fracture surfaces are reported in Fig. 1. Most of the spinel matrix grains of the composites hot-pressed at 1200 and 1300 °C (Fig. 1a–d) have a diameter smaller than 100 nm and form larger agglomerates, similarly to what can be observed in the starting powder (Fig. 2d). By contrast, most grains have grown in the composite hot-pressed at 1500 °C, some reaching more than 500 nm (Fig. 1g–h), while at 1400 °C only some matrix grains seem to have grown (Fig. 1e and f). We also observe many CNT (or CNT bundles) that have not been broken, or have been broken after some pull-out, whereas CNT that may have been broken at the level of the fracture surface cannot be observed. For each hot-pressing temperature, the observations conducted in many areas and on several specimens, show that CNT (or CNT bundles) are always evidenced, in agreement with their very homogeneous distribution within the composite powders (Fig. 2d). However, it appeared also that many CNT have been damaged in the composite hot-pressed at 1500 °C, and also in a lesser extend in that hot-pressed at 1400 °C, producing some short CNT residues or carbon clusters at the grain boundaries and grain junctions of the matrix (Figs. 1h, 1f). As a result of this preliminary study, 1300 °C was thought to be a low enough temperature so as to not damage the CNT and therefore was chosen as the hot-pressing temperature for the rest of the work.

3.2. Influence of the content of carbon nanotubes

Typical FEG-SEM images of composite powders, revealing the increasing quantity of CNT, are shown in Fig. 2. These images show also some differences in the microstructure of the matrix grains. The C powders (Fig. 2a and b) contain relatively

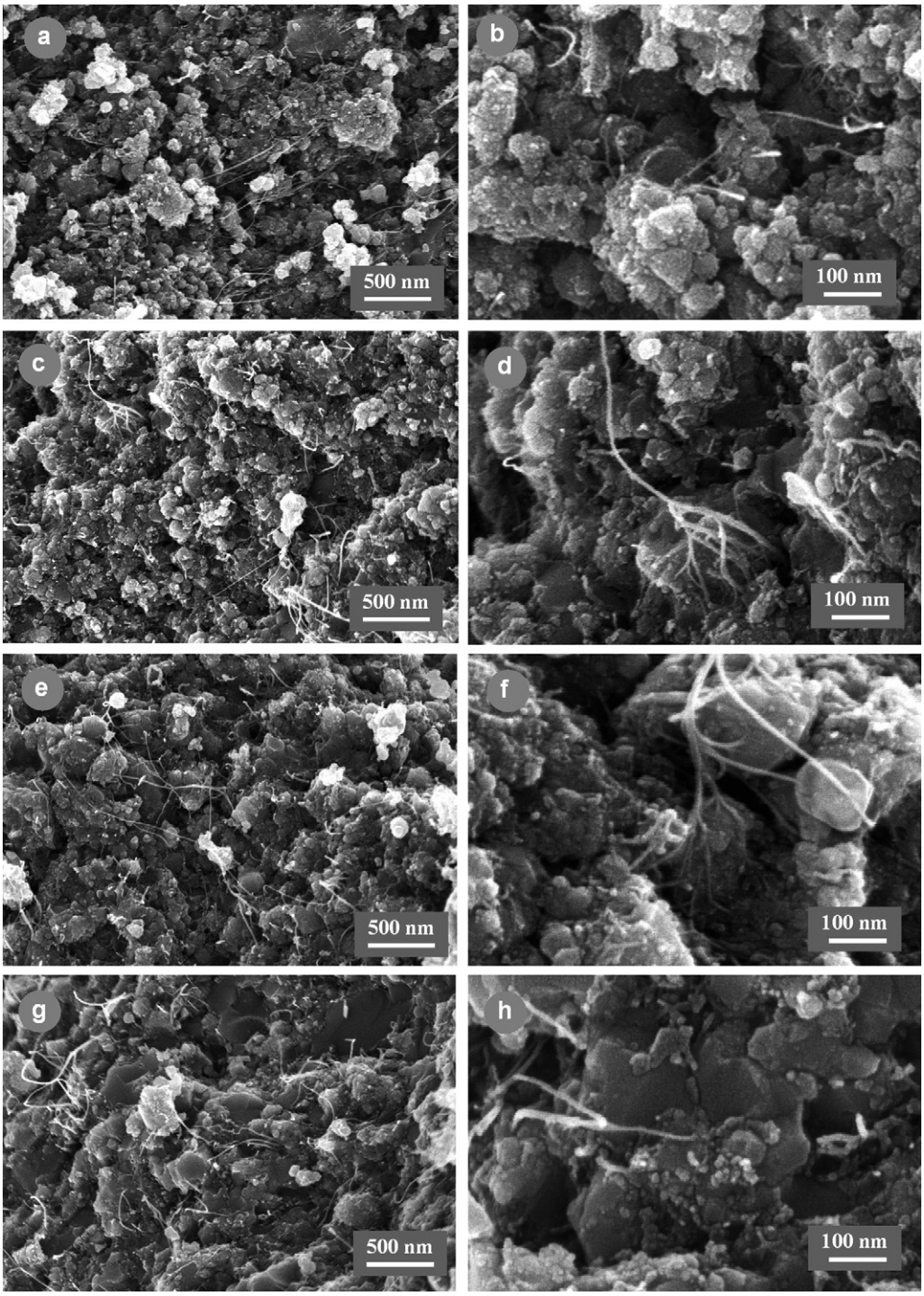

Fig. 1. FEG-SEM images of the fracture surfaces of the 15.5 vol.% CNT–Co/Mo–$MgAl_2O_4$ composite (specimen CM7) hot-pressed at different temperatures: (a and b) 1200 °C; (c and d) 1300 °C; (e and f) 1400 °C; (g and h) 1500 °C.

non-porous grains (up to 500 nm large) which are made up of well sintered primary grains, some of these large grains having a plate-like form. The CM powders (Fig. 2c and d) contain porous agglomerates of much smaller grains (generally less than 100 nm). This difference is consistent with the specific surface area of the solid solution powders before reduction which are around 20 and 40 m^2/g, for C and CM powders, respectively. In all powders, the CNT network forms a very well distributed interconnected web. In C powders, this web is formed of filaments with small diameters, most being probably individual CNT (Fig. 2a and b) whereas, in CM powders (Fig. 2c and d), this web is very dense and formed of bundles, up to 10–20 nm in diameter, made up of several CNT. The specimens do not contain any large MWNT, carbon fibres nor disordered carbon. Statistical studies on HRTEM images have shown that 70–90% of the CNT are SWNT, most of the others being DWNT. The

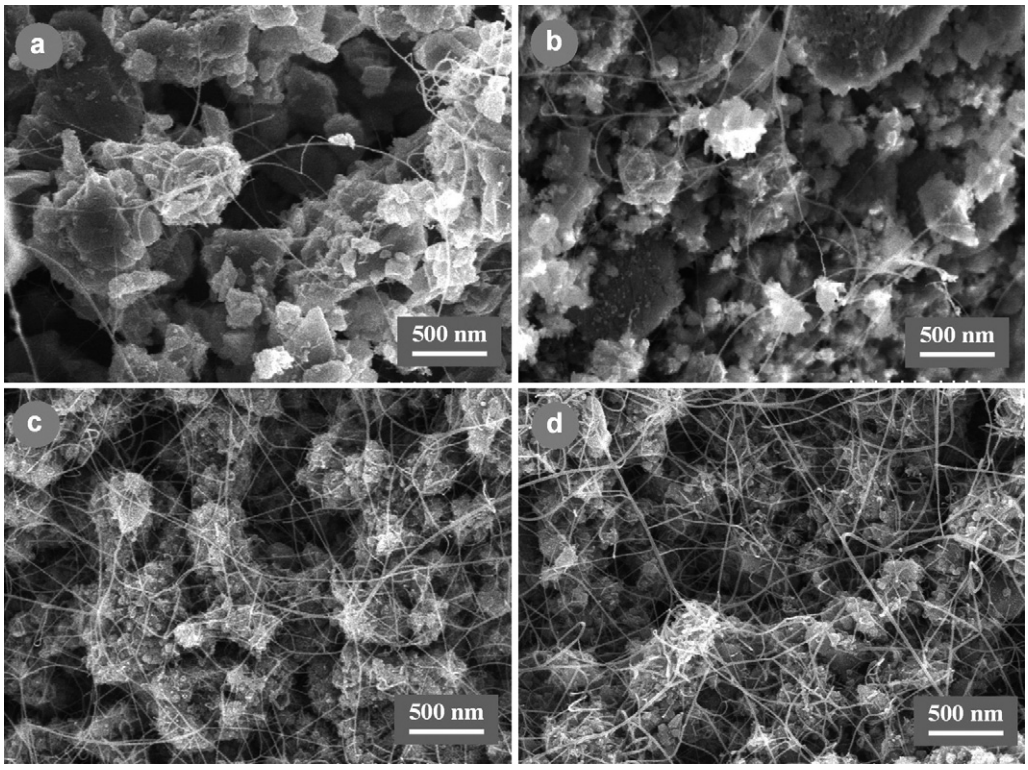

Fig. 2. FEG-SEM images of some CNT–Co/Mo–$MgAl_2O_4$ composite powders: (a) specimen C1, (b) specimen C3, (c) specimen CM1 and (d) specimen CM7.

CNT diameter is in the 0.5–5 nm range with a mean diameter between 2.4 and 2.8 nm. From these common characteristics, a CNT density of 1.70 was calculated and was used to calculate the CNT vol.% from the experimental CNT in wt% (Table 3). X-ray diffraction revealed the presence of ε-Co besides the $MgAl_2O_4$ matrix in all specimen and of some Mo_2C in CM specimens. From the chemical composition of the starting catalytic materials, taking into account that the reduction of Co^{2+} in Co^0 was complete,[30] we have deduced the volume contents in ε-Co and Mo_2C (Table 3) and it is noted that the values are not higher than 3.08 and 2.47 vol.%, respectively. Calculations showed that the carbon contained in Mo_2C is negligible when compared to that in the CNT.

The green densification (Table 3 and Fig. 3a) of the C specimen tends to decrease, from 52 to 49%, when the CNT content is increased from 1.2 to 7.7 vol.%. The CM specimens (CNT content from 9.4 to 16.7 vol.%) have a green densification around 45%, lower than that of the C specimens, except specimen CM7 whose higher than expected green densification was caused by a pressure exceeding 100 MPa during the cold-pressing. The hot-pressed densification for specimen containing more than 5 vol.% of CNT (Table 3 and Fig. 3b) regularly decreases when the CNT

Table 3
Characteristics of the CNT–metal–$MgAl_2O_4$ composites hot-pressed at 1300 °C: Co and Mo_2C contents (vol.%) calculated from the composition of the specimen; C_n and C_v, the measured carbon content (wt.%) and the corresponding calculated carbon content (vol.%) taken as the CNT content; green d, green densification; HP d, hot-pressed densification

Specimen	Co (vol.%)	Mo_2C (vol.%)	C_n (wt.%)	C_v (vol.%)	Green d (%)	HP d (%)
C1	0.32	0	0.55	1.2	51.9 ± 1.3	100.0 ± 2.6
C2	1.93	0	0.6	1.3	51.8 ± 1.3	99.8 ± 2.5
C3	2.31	0	1.4	2.5	50.0 ± 1.3	99.7 ± 2.5
C4	3.14	0	2.5	5.3	48.8 ± 1.2	98.3 ± 2.5
C5	3.13	0	2.6	5.5	49.0 ± 1.2	95.6 ± 2.4
C6	3.08	0	3.7	7.7	49.4 ± 1.2	92.7 ± 2.3
CM1	1.51	1.30	4.4	9.4	44.9 ± 1.1	86.6 ± 2.2
CM2	2.86	2.47	5.1	11.2	43.5 ± 1.1	83.8 ± 2.1
CM3	2.89	1.25	6.4	12.2	45.4 ± 1.1	81.0 ± 2.0
CM4	2.79	2.41	7.0	15.1	42.4 ± 1.1	76.9 ± 1.9
CM5	1.44	1.25	7.2	15.0	45.3 ± 1.1	76.6 ± 1.9
CM6	2.78	2.40	7.3	15.7	43.7 ± 1.1	76.2 ± 1.9
CM7	0.73	1.25	7.5	15.5	49.0 ± 1.2	80.2 ± 2.1
CM8	2.83	1.22	7.8	16.3	43.8 ± 1.1	76.2 ± 1.9
CM9	2.82	1.22	8.0	16.7	45.6 ± 1.1	73.4 ± 1.8

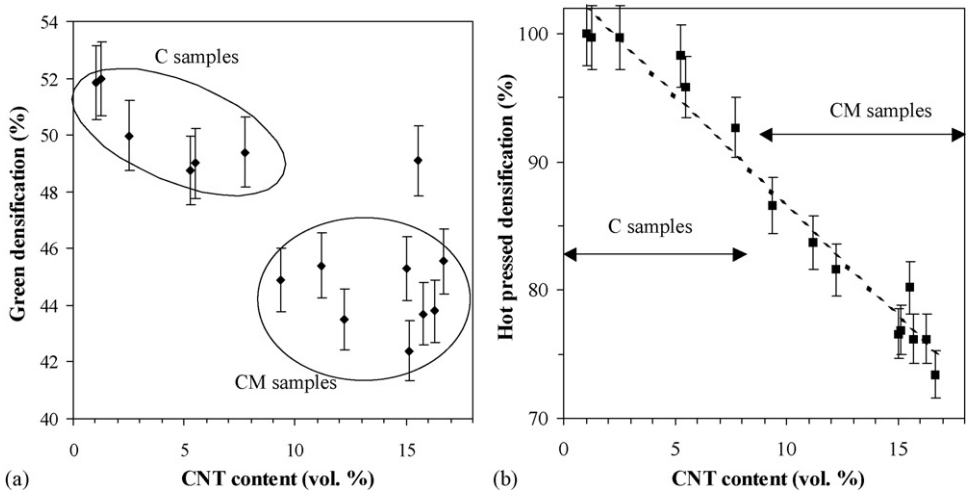

Fig. 3. Green densification (a) and hot-pressed densification (b) vs. the CNT content in the hot-pressed CNT–Co/Mo–$MgAl_2O_4$ composites.

content increases, reaching only 73.4% for CM9 (16.7 vol.% CNT). The relative shrinkage versus temperature for the C composites, prepared using only cobalt as a catalytic metal, is shown in Fig. 4a and b. For these specimens, the shrinkage curves have similar shapes and, when the CNT content increases, they differ only by slight shifts towards lower temperatures and some variations in shrinkage slopes. To permit a comparison between the shrikage slopes, we divided the curves in three ranges (Fig. 4a and b), firstly between 900 °C and T_1, secondly between T_1 and T_2 and thirdly between T_2 and 1300 °C. The transition temperatures were chosen at values at which the shrinkage is no more almost linear, but notably increases at T_1 and notably decreases at T_2. Possibly, changes in the dominant mechanism occur at these temperatures, but that could be confirmed only by further studies related to the kinetic of shrinkage. For each of the C specimen, the values of T_1 and T_2 are reported in Table 4. For increasing CNT contents, both tend to decrease (from 1070 to 1030 °C and from 1220 to 1170 °C, respectively). We calculated that at these temperatures, the C specimens have similar relative densities, respectively, equal to (60.0 ± 0.5%) and (82 ± 1%). The shrinkage slopes in each of the three ranges, obtained by a linear fitting, are reported in Table 4. Note that since the heating rates are constant (10 ± 1 °C/min) the comparisons of the shrinkage slopes (%/°C) are representative of that of the shrinkage rates (%/min), but we keep the slope as the parameter to avoid any confusion with isothermal studies.

It is well known that, in the first step of hot-pressing, the shrinkage is mainly due to particle rearrangement towards more dense packing.[31] We infer that for the present C specimen, this mechanism is the dominant one in the range 1. It normally leads to a relative density around 60%[31] which is effectively obtained at T_1. In spite of the initial cold-pressing operated at 100 MPa, some rearrangement could occur at 900–1050 °C under 43 MPa because the green relative densities are still low (Table 3) and the thermal expansion upon heating creates internal stresses in the packing which can facilitate the mobility of particles. For increasing CNT contents, the shrinkage slope of the C specimen tends to increase (Table 4 and Fig. 5a). The end

Table 4
Shrinkage slope (%/°C) in different temperature ranges for C and CM specimen hot-pressed at 1300 °C

Specimen	C_n (vol.%)	T_1 (°C)	T_2 (°C)	Shrinkage slopes (%/°C)		
				Range 1, 900–T_1 (°C)	Range 2, T_1–T_2 (°C)	Range 3, T_2–1300 (°C)
C1	1.2	1070	1220	0.084 ± 0.006	0.178 ± 0.010	0.095 ± 0.005
C2	1.3	1070	1220	0.089 ± 0.006	0.170 ± 0.010	0.081 ± 0.005
C3	2.5	1050	1180	0.086 ± 0.006	0.184 ± 0.010	0.084 ± 0.005
C4	5.3	1050	1170	0.104 ± 0.006	0.181 ± 0.010	0.077 ± 0.005
C5	5.5	1030	1170	0.093 ± 0.006	0.178 ± 0.010	0.079 ± 0.005
C6	7.7	1030	1170	0.099 ± 0.006	0.155 ± 0.010	0.069 ± 0.005
CM1	9.4	1060	1160	0.108 ± 0.007	0.134 ± 0.011	0.100 ± 0.006
CM2	11.2	1100	1180	0.096 ± 0.008	0.131 ± 0.012	0.095 ± 0.007
CM3	12.2	1100	1180	0.093 ± 0.009	0.116 ± 0.013	0.087 ± 0.008
CM4	15.1	–	–	0.084 ± 0.006		
CM5	15.0	–	–	0.073 ± 0.006		
CM6	15.7	–	–	0.078 ± 0.006		
CM7	15.5	–	–	0.091 ± 0.006		
CM8	16.3	–	–	0.074 ± 0.006		
CM9	16.7	–	–	0.071 ± 0.006		

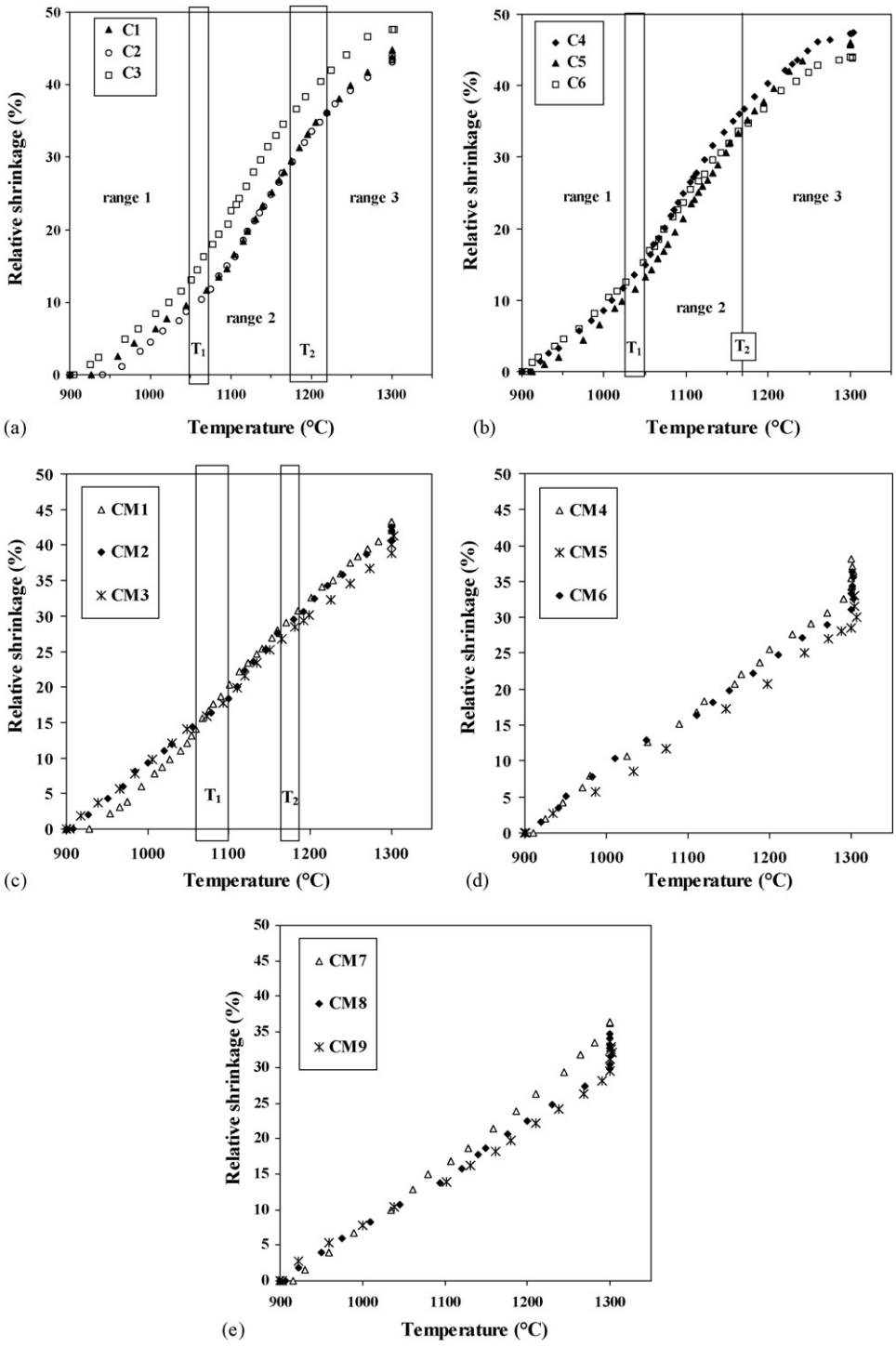

Fig. 4. Relative shrinkage vs. temperature for all CNT–Co/Mo–$MgAl_2O_4$ composites: (a) specimen C1–C3, (b) specimen C4–C6, (c) specimen CM1–CM3, (d) specimen CM4–CM6 and (e) specimen CM7–CM9.

temperature (T_1) of the first step decreases from 1070 to 1030 °C (Table 4) because the temperature at which the relative density of 60% is reached decreases when the shrinkage slope increases. It has been shown that, at room temperature, an increase content of CNT in a ceramic matrix composite lower the coefficient of friction,[7,14] either by the action of rolling or slidding.[7] In the present composite powders, a lot of CNT and CNT bundles are located between matrix grains. So it is reasonable to infer that CNT facilitate the sliding at grain contacts, explaining the notable increase of the shrinkage slope with the CNT content.

For higher densifications, i.e. above T_1, the shrinkage slope increases because another mechanism may possibly become predominant. The second step of hot-pressing is usually the shrinkage of the open channel porosity via plastic flow and/or lattice diffusion[31] and leads to a relative density around 90%. In

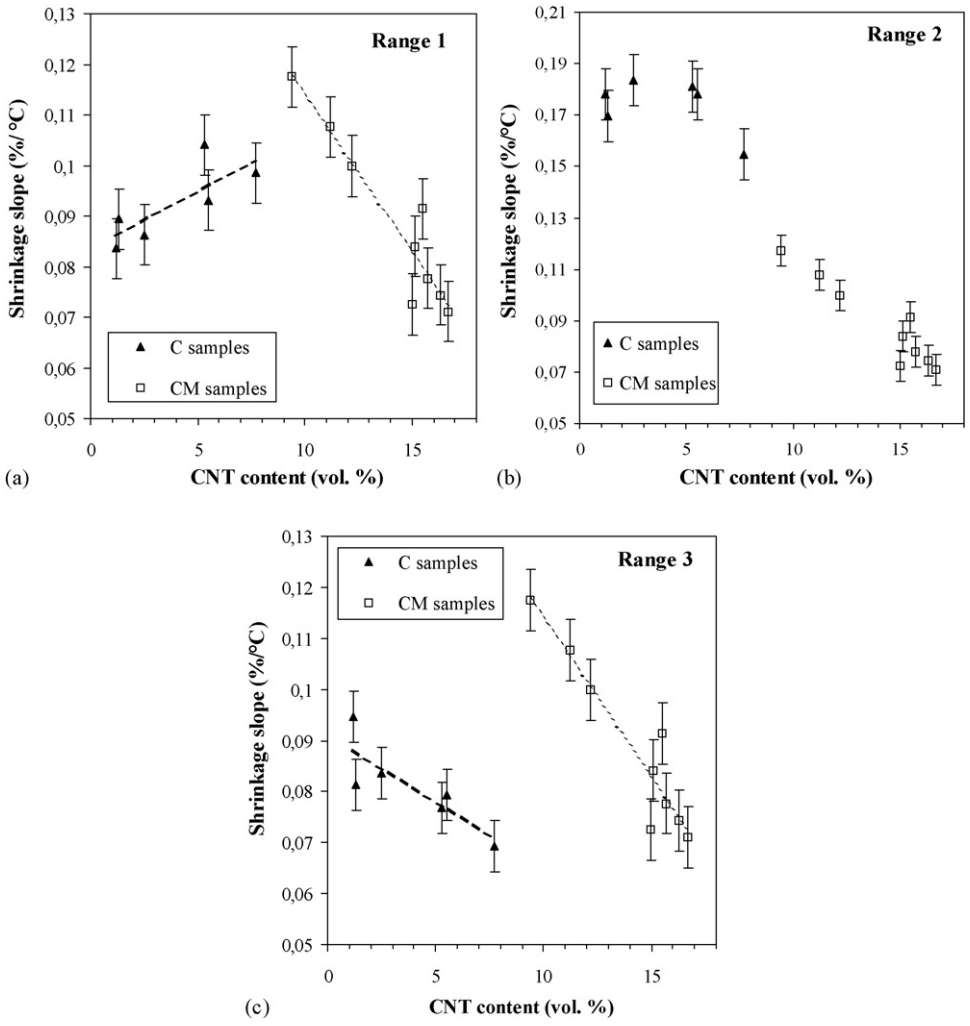

Fig. 5. Shrinkage slope vs. the CNT content of the hot-pressed CNT–Co/Mo–$MgAl_2O_4$ composites for different temperature ranges: (a) 900C–T_1, (b) T_1–T_2 and (c) T_2–T_3. For C specimen and CM1–CM3 specimen, the values of T1 and T2 are reported in Table 4. For C1–C6 and CM1–CM3 specimen, the shrinkage slopes were obtained by linear fitting of the curve shrinkage vs. temperature, in each of the three ranges. For CM4–CM9 specimen, the shrinkage slopes were obtained by a unique linear fitting between 900 and 1300 °C.

the present work, a densification of only (82 ± 1%) is reached at the end of range 2 showing that the shrinkage of the open channel porosity continues during a part of range 3. For the C specimens, as a function of the CNT content (Table 4), the shrinkage slopes in the ranges 2 and 3 (Fig. 5b) begin to decrease clearly only for C6 (7.7 vol.%). To assess a dominant mechanism during the second step of hot-pressing, the values of the pressure, the temperature and the particle size must be considered.[31] In our case, if the pressure is moderate and the particle are of submicrometric size, which speaks in favour of boundary and/or lattice diffusion, the temperature is also rather low which speaks in favour of plastic flow. Using powders of 0.13–0.15 μm particle size and moderate applied pressures (5–38 MPa), Ting and Lu[32,33] studied the rate-determining mechanism involved in the hot-pressing of $MgAl_2O_4$ as a function of the stoichiometry. They showed that the Nabarro–Herring diffusion creep dominates the densification in low stress regimes. They also showed that the transition stress at which the mechanism changes from diffusion creep to dislocation creep is lower when the spinel has an excess of Al_2O_3, in agreement with the variation the concentration of oxygen vacancy which controls the lattice diffusion.

In the present composite specimens, because Co^{2+} ions present in the starting solid solution have been reduced to the metallic state, the resulting $MgAl_2O_4$ is not stoechiometric but rather with an an excess of Al_2O_3.[30] This excess increases from C1 to C4, in relation with the increasing Co^{2+} content in the starting solid solution (from 1 to 20 cat.%—Table 1). In comparison with the works of Ting and Lu,[32,33] the present specimens contain a relatively large excess of Al_2O_3, we use a slight higher pressure (43 MPa versus 38 MPa) and lower temperatures (900–1300 °C versus 1450 or 1550 °C). So, it is difficult to settle between the two dominant mechanisms proposed by Ting and Lu.[32,33] Some ε-Co nanoparticles are located at the surface of spinel grains and they could act on the shrinkage mechanism. From the specimens C1 to C5, in spite of the fact that both ε-Co and the CNT contents increase (from 0.32 to 3.13 vol.% and from 1.2 to 5.5 vol.%, respectively), the shrinkage remains constant (Table 4 and Fig. 5b). Thus, within these content ranges, neither

ε-Co nanoparticles nor CNT influence the kinetic of the dominant mechanism. In comparison to C5, the C6 specimen contains a similar quantity of ε-Co but a clearly higher quantity of CNT, resulting in lower shrinkage slopes in ranges 2 and 3 (Fig. 5b and c), without shifts of the transition temperatures (Table 4). Thus, it appears that, when their amount become sufficient (7.7 vol.% for C6), CNT clearly inhibit the shrinkage mechanisms involved in ranges 2 and 3.

The CM specimens will now be considered. They differ from each other firstly (and mainly) by the CNT content, secondly (but to a lesser extent) by the Al_2O_3 excess in the spinel and thirdly by the ε-Co and Mo_2C contents (Table 3). Only CM1, CM2 and CM3 specimen have relative shrinkage curves (Fig. 4c) made up of three steps similar to those of the C specimens (Fig. 4a and b), but with a narrower range 2, beginning at a higher temperature T_1 and ending at a lower temperature T_2 (Table 4). The densification at T_1 is around 59, 62 and 64% for CM1, CM2 and CM3, respectively, not very far from that of the C specimens at T_1 (around 60%). For CM4–CM9, the shrinkage is clearly almost linear from 900 to 1300 °C (Fig. 4d and e and Table 4) and continues during the dwell time at 1300 °C, in contrast with the C specimens (Fig. 4a and b). This is consistent with the low densification achieved (70–80%) at the beginning of the dwell time at 1300 °C. The shrinkage slopes for the CM specimens are plotted on the same graphs as those of the C specimen versus the CNT content (Fig. 5a–c). For CM specimen, in each of the three temperature ranges, the trend is clearly that the slope decreases when the CNT content increases. In the range 1, CM1–CM3 specimen have a slightly higher or similar shrinkage slope than that of C4–C6 (Fig. 5a). But in contrast to what is observed for the C specimens, the slope decreases with the CNT content, from CM1 to CM9 (Fig. 5a). It is well known that CNT have a very high Young modulus. Moreover, in the CM samples, they form a dense web-like structure extensively branched all around the matrix grains (Fig. 3c and d). This web-like structure is detrimental to the mobility of the matrix grains and the rearrangement is probably notably hindered. This phenomenon would be all the more pronounced when the CNT web is more interconnected and more dense, i.e. when the quantity of CNT is increased, from CM1 to CM9.

In range 2, the shrinkage slopes are lower for CM specimens than for C specimens (Fig. 5b) and clearly tend to decrease when the CNT content increases. In range 3, the shrinkage slopes are lower for the CM than for the C specimens (Fig. 5b) and clearly tend to decrease when the CNT content increases. In spite of the fact that CM samples differ also, one from the other, by their Al_2O_3 excess, their ε-Co and their Mo_2C contents, the inhibition of the shrinkage shows a good correlation only with the regular increasing quantity of CNT from CM1 to CM9. Thus, the study of the CM specimens confirms that CNT over 5 vol.%, greatly inhibit the densification mechanism(s). As will be confirmed below, the matrix grain growth stays, at this stage, almost ineffective. Consequently, most CNT are still located at grain boundaries, and thus cannot directly inhibit the creep within the matrix grain, as can usually do precipitated second phase particles. A possible explanation is a mechanical role of the CNT which could redistribute the stresses in transversal directions, decreasing the shear stresses in the longitudinal direction and thus inhibiting the dislocation creep, if this mechanism is dominant. Ting and Lu[32,33] point out that for compositions with an excess of Al_2O_3, the relative density can reach a plateau. This could explain the progressive lowering of the shrinkage slope from T_2 to 1300 °C for C and CM1–CM3 specimens. In contrast, this plateau of relative density would not be reached for CM4–CM9 specimens which could explain that the shrinkage remains linear up to 1300 °C (Table 4 and Fig. 5b and c).

High resolution SEM images of the fracture surface of some hot-pressed specimen are shown in Fig. 6. The C2 specimen (Fig. 6a), which contain only 1.3 vol.% CNT, presents a mainly transgranular fracture mode, which is characteristic of metal–ceramic nanocomposites, when many metal nanoparticles are located within the matrix grains. In this sample, most grains are larger than 200 nm and the smaller grains of the powder (Fig. 1a and b) are not observed anymore in the hot-pressed specimen. A significant grain growth has occurred and allowed the complete elimination of the discontinuous porosity (relative densifity of 99.8%—Table 3). The fracture surface of C6 (Fig. 6b), which contains 7.7 vol.% CNT, is somewhat different from that of C2. Many grains are smaller than 200 nm, some being not larger than 10–20 nm. These nanometer grains perhaps correspond to the ε-Co nanoparticles which have been covered by carbon capsules during the CNT synthesis. The fact that these particles kept their nanometer size suggests that they did not reached the liquid state during the hot-pressing. Some pores are observed and their size is of the order of the larger matrix grains, which is consistent with the uncompleted elimination of the discontinuous porosity (relative density of 92.7%—Table 3). Only some CNT are observed on the fracture surface of C2 and C6 but the amount of CNT in the composites CNT is under-estimated on the images. The reason is that most of CNT, and particularly those which are at intragranular positions, have been broken at the level of the fracture surface and cannot be seen on SEM images. On the fracture surface of CM3 and CM4 (Fig. 6c and d), which contain 12.2 and 15.1 vol.% CNT, respectively, much more CNT are observed because of the inherently higher content but also because many CNT, located in the large pores, have not been broken. The fracture of these specimens is mainly intergranular because the matrix grains are much smaller than that of C2 or C6 specimens. Only some grains reach 200 nm in CM3 (Fig. 6c) and a lot of primary grains of the agglomerates in the powder still remain in the hot-pressed specimen, particularly in CM4. As expected from the relative densities (81.0 and 76.9% for CM3 and CM4, respectively) and the shape of the shrinkage curves (Fig. 4c and d), many large pores which belong to the open channel porosity and are located between the agglomerates have not been eliminated.

Using hot-pressing at higher temperatures (1450–1500 °C), it was shown that the inhibition of matrix grain growth usually provoked by the presence of metal nanoparticles is enhanced by the CNT.[20] The elimination of the larger pores can thus not be effective, resulting in an unsufficient densification.[20] However, some diffusion mechanisms operate at these higher temperatures, as shown by a significant begining of grain growth. Thus, CNT located at the grain boundary probably inhibit the mobility

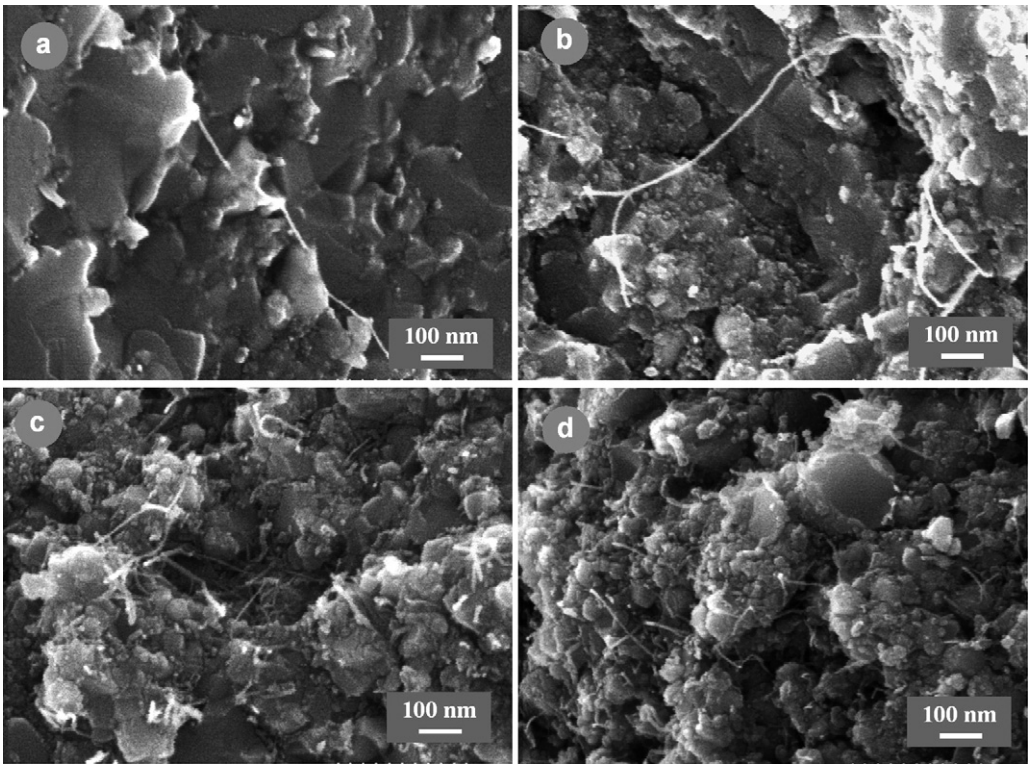

Fig. 6. FEG-SEM images of the fracture surfaces of some CNT–Co/Mo–$MgAl_2O_4$ composite hot-pressed at 1300 °C: (a) specimen C2, (b) specimen C6, (c) specimen CM3 and (d) specimen CM4.

of the grain boundaries, as usally do precipitated second phase particles. Consequently, increasing the hot-pressing temperature too much is not efficient and, in any case, a moderate temperature is preferable to stay at in order to prevent the damaging of CNT. A better solution would be a higher applied pressure, firstly to crush the matrix grain agglomerates, secondly to obtain a higher efficiency of the plastic flow. Finally, the microstructure of the green sample has to be optimised, particularly to avoid the presence of large inter-agglomerate pores. These pores are much more difficult to eliminate at moderate pressure when the specimen contains a great quantity of CNT which, owing to their high rigidity, decrease the shear stresses within the compact.

Zhan et al.[5] have shown that CNT–Al_2O_3 composites prepared by mechanical mixing of CNT and nanometric Al_2O_3 powder can be well densified by the spark plasma sintering technique. This technique allows the use of a nanometric Al_2O_3 powder, which is beneficial to the quality of the green specimen. But the disadvantages are a lesser homogeneous distribution of CNT and certainly significant damages to CNT during the very long ball-milling step.[5] We proposed that a part of the detrimental influence of CNT on the densification could be due to their exceptional mechanical properties. So, signicant damages to CNT, detrimental to their rigidity, and a lesser distribution of CNT within the matrix probably favour a better densification on hot-pressing or upon SPS. However, the use of the SPS technique allows to sinter in very short times, limiting the matrix grain growth and probably the damaging of CNT. The first works of the present authors using the SPS technique to sinter CNT–metal oxide nanocomposites with high CNT contents have shown that, in comparison to hot-pressing, the relative density is increased but not up to the theoretical density. It appears also that applied pressures higher than 43 MPa (i.e. 100 or 150 MPa) are preferable. However, the use of nanometric and non-agglomerated matrix powders, which allows to prepare green specimens having a microstructure more favourable to the densification, is also useful.

4. Conclusions

A study of the densification by hot-pressing of ceramic–matrix composites containing a dispersion of CNT (70–90% being SWNT and most of the others being DWNTs) is proposed for the first time. A family of 15 different CNT–Co/Mo–$MgAl_2O_4$ composite powders containing between 1.2 and 16.7 vol.% CNT was prepared by CCVD. The in situ growth of CNT within the oxide powder permitted to obtain a highly homogeneous distribution of the CNT which forms a web-like structure all around the matrix grains. The hot-pressing was performed under 43 MPa at a constant heating rate of 10 °C/min. A preliminary study led to limit the maximum temperature at 1300 °C to prevent CNT damages. The influence on sintering of the CNT and that of other microstructural characteristics of the starting materials were discriminated. At low contents (below 6 vol.%), CNT are beneficial to the rearrangement process involved in the first shrinkage step. We proposed that CNT have a lubricating role which facilitates the sliding at grain contacts or boundaries. But, at higher contents, CNT inhibit this process. We proposed that, for this CNT contents, their web-like

structure becomes very well interconnected, very rigid, and thus inhibits the rearrangement process. During the second shrinkage step, CNT clearly inhibit the shrinkage, and this detrimental effect regularly increases with the CNT content. Although it was not possible to settle precisely to the involved mechanism, we proposed that CNT decrease the shear stresses in the longitudinal direction, redistribute the stresses in transversal directions, thus inhibiting the plastic flow. Higher applied pressures could be efficient to compensate this detrimental effect. At higher temperatures, the shrinkage mechanism would involve some grain growth but CNT tend to be damaged. Moreover, previous studies have shown that at these stages, CNT inhibit the grain growth probably because they inhibit the mobility of the grain boundaries, as usually do precipitated second phase particles. Thus, hot-pressing at higher temperatures is not efficient to fully densify the present materials. Preliminary works showed that the use of spark plasma sintering lead to a better densification of the present materials.

References

1. Laurent, C. and Peigney, A., Carbon nanotubes in composite materials. In *Encyclopedia of Nanoscience and Nanotechnology*, ed. H. S. Nalwa. Am. Sci. Pub., 2004, pp. 635–653.
2. Peigney, A. and Laurent, C., Carbon nanotubes ceramic composites. In *Ceramic Matrix Composites: Microstructure–Property Relationship*, ed. I. M. Low. Woodhead Publishing Limited, Cambridge, England, 2006, pp. 309–333.
3. Ma, R. Z., Wu, J., Wei, B. Q., Liang, J. and Wu, D. H., Processing and properties of carbon nanotube/nano-SiC ceramic. *J. Mater. Sci.*, 1998, **33**, 5243–5246.
4. Ning, J., Zhang, J., Pan, Y. and Guo, J., Fabrication and mechanical properties of SiO_2 matrix composites reinforced by carbon nanotube. *Mater. Sci. Eng. A: Struct. Mater. Prop. Microstruct. Process.*, 2003, **A357**, 392–396.
5. Zhan, G.-D., Kuntz, J. D., Wan, J. and Mukherjee, A. K., Single-wall carbon nanotubes as attractive toughening agents in alumina-based nanocomposites. *Nat. Mater.*, 2003, **2**, 38–42.
6. Wang, X., Padture, N. P. and Tanaka, H., Contact-damage-resistant ceramic/single-wall carbon nanotubes and ceramic/graphite composites. *Nat. Mater.*, 2004, **3**, 539–544.
7. Lim, D. S., You, D. H., Choi, H. J., Lim, S. H. and Jang, H., Effect of CNT distribution on tribological behavior of alumina–CNT composites. *Wear*, 2005, **259**, 1–6 (Part 1 Special Issue SI, 539–544).
8. Fan, J., Zhao, D., Wu, M., Xu, Z. and Song, J., Preparation and microscrucrture of multi-wall carbon nanotubes-toughened Al_2O_3 composite. *J. Am. Ceram. Soc.*, 2006, **89**, 750–753.
9. Peigney, A., Laurent, C., Dobigeon, F. and Rousset, A., Carbon nanotubes grown in situ by a novel catalytic method. *J. Mater. Res.*, 1997, **12**, 613–615.
10. Laurent, C., Peigney, A. and Rousset, A., Synthesis of carbon nanotube–Fe–Al_2O_3 nanocomposite powders by selective reduction of different $Al_{1.8}Fe_{0.2}O_3$ solid solutions. *J. Mater. Chem.*, 1998, **8**, 1263–1272.
11. Govindaraj, A., Flahaut, E., Laurent, C., Peigney, A., Rousset, A. and Rao, C. N. R., An investigation of carbon nanotubes obtained from the decomposition of methane over reduced $Mg_{1-x}M_xAl_2O_4$ spinel catalysts. *J. Mater. Res.*, 1999, **14**, 2567–2576.
12. Flahaut, E., Govindaraj, A., Peigney, A., Laurent, C., Rousset, A. and Rao, C. N. R., Synthesis of single-walled carbon nanotubes using binary (Fe, Co, Ni) alloy nanoparticles prepared in situ by the reduction of oxide solid solutions. *Chem. Phys. Lett.*, 1999, **300**, 236–242.
13. Flahaut, E., Peigney, A., Laurent, C. and Rousset, A., Synthesis of single-walled carbon nanotube–Co–MgO composite powders and extraction of the nanotubes. *J. Mater. Chem.*, 2000, **10**, 249–252.
14. An, J. W., You, D. H. and Lim, D. S., Tribological properties of hot-pressed alumina–CNT composites. *Wear*, 2003, **255**, 677–681.
15. Liu, Y. Q. and Gao, L., A study of the electrical properties of carbon nanotube–$NiFe_2O_4$ composites: effect of the surface treatment of the carbon nanotubes. *Carbon*, 2005, **43**, 47–52.
16. Mo, C. B., Cha, S. I., Kim, K. T., Lee, K. H. and Hong, S. H., Fabrication of carbon nanotube reinforced alumina matrix nanocomposite by sol–gel process. *Mater. Sci. Eng. A: Struct. Mater. Prop. Microstruct. Process.*, 2005, **A395**, 124–128.
17. Huang, Q. and Gao, L., Manufacture and electrical properties of multiwalled carbon nanotube/$BaTiO_3$ nanocomposite ceramics. *J. Mater. Chem.*, 2004, **14**, 2536–2541.
18. Laurent, C., Peigney, A., Dumortier, O. and Rousset, A., Carbon nanotubes Fe alumina nanocomposites. Part II. Microstructure and mechanical properties of the hot-pressed composites. *J. Eur. Ceram. Soc.*, 1998, **18**, 2005–2013.
19. Peigney, A., Laurent, C., Flahaut, E. and Rousset, A., Carbon nanotubes in novel ceramic matrix nanocomposites. *Ceram. Int.*, 2000, **26**, 677–683.
20. Flahaut, E., Peigney, A., Laurent, C., Marliere, C., Chastel, F. and Rousset, A., Carbon nanotube–metal–oxide nanocomposites: microstructure, electrical conductivity and mechanical properties. *Acta Mater.*, 2000, **48**, 3803–3812.
21. Rul, S., Lefevre-schlick, F., Capria, E., Laurent, C. and Peigney, A., Percolation of single-walled carbon nanotubes in ceramic matrix nanocomposites. *Acta Mater.*, 2004, **52**, 1061–1067.
22. Zhan, G.-D., Kuntz, J. D., Garay, J. E. and Mukherjee, A. K., Electrical properties of nanoceramics reinforced with ropes of single-walled carbon nanotubes. *Appl. Phys. Lett.*, 2003, **83**, 1228–1230.
23. Sun, J., Gao, L. and LI, W., Colloidal processing of carbon nanotube/alumina composites. *Chem. Mater.*, 2002, **14**, 5169–5172.
24. Chan, M. O. B., Seung, C. H. A. I., Kyung, K. I. M. T., Kyung, L. E. E. H. and Hong, S. H., Fabrication of carbon nanotube reinforced alumina matrix nanocomposite by sol–gel process. *Mater. Sci. Eng. A: Struct. Mater. Prop. Microstruct. Process.*, 2005, **395**, 124–128.
25. Kingsley, J. J. and Patil, K. C., A novel combustion process for the synthesis of fine a-alumina and related oxide materials. *Mater. Lett.*, 1998, **6**, 427–432.
26. Rul, S., Peigney, A., Bacsa, W. S. and Laurent, C., Ceramic foams for the CCVD synthesis of single-walled carbon nanotubes. 2006, submitted for publication.
27. Flahaut, E., Bacsa, R., Peigney, A. and Laurent, C., Gram-scale CCVD synthesis of double-walled carbon nanotubes. *Chem. Com.*, 2003, 1442–1443.
28. Flahaut, E., Peigney, A., Bacsa, W. S., Bacsa, R. R. and Laurent, C., CCVD synthesis of carbon nanotubes from (Mg, Co, Mo)O catalysts: influence of the proportions of cobalt and molybdenum. *J. Mater. Chem.*, 2004, **14**, 646–653.
29. Rul, S., Laurent, C., Peigney, A. and Rousset, A., Carbon nanotubes prepared in situ in a cellular ceramic by the gelcasting-foam method. *J. Eur. Ceram. Soc.*, 2003, **23**, 1233–1241.
30. Quenard, O., Laurent, C., Brieu, M. and Rousset, A., Synthesis, microstructure and oxidation of Co–$MgAl_2O_4$ and Ni–$MgAl_2O_4$ nanocomposites powders. *Nanostruct. Mater.*, 1996, **7**, 497–507.
31. Coble, R. L., Mechanisms of Densification During Hot Pressin. In *Sintering and Related Phenomena*, ed. G. C. Kuczynski, N. A. Hooton and C. F. Gibbon. Gordon and Breach, New York, 1967, pp. 329–350.
32. Ting, C. J. and Lu, H. Y., Hot-pressing of magnesium aluminate spinel. I. Kinetics and densification mechanism. *Acta Mater.*, 1999, **47**, 817–830.
33. Ting, C. J. and Lu, H. Y., Hot-pressing of magnesium aluminate spinel. II. Microstructure development. *Acta Mater.*, 1999, **47**, 831–840.